III International Conference on Particle-based Methods – Fundamentals and Applications
PARTICLES 2013
M. Bischoff, E. Oñate, D.R.J. Owen, E. Ramm & P. Wriggers (Eds)

THE APPLICATION OF COUPLED FINITE-DISCRETE ELEMENT METHOD IN ANALYZING SOIL-STRUCTURE INTERACTION PROBLEMS

Viet D.H. Tran [1], Mohamed A. Meguid[2*], and Luc E. Chouinard[3]

[1] Graduate student
Department of Civil Engineering and Applied Mechanics, McGill University, Canada
Email address: viet.tran@mail.mcgill.ca

[2*] Associate Professor
Department of Civil Engineering and Applied Mechanics, McGill University, Canada
Email address: mohamed.meguid@mcgill.ca

[3] Associate Professor
Department of Civil Engineering and Applied Mechanics, McGill University, Canada
Email address: luc.chouinard@mcgill.ca

*Corresponding author

Key words: Discrete element, Finite-Discrete element, soil-structure interaction, geogrid modeling.

Abstract. A framework to couple the Finite and the Discrete element methods is proposed in this study. The framework takes advantage of both approaches to investigate different soil-structure interaction problems. The structural elements in the problems are modeled using finite elements whereas surrounding soil is modeled using discrete elements to reflect the discontinuous nature of the granular material. The coupled framework is then used to model three soil-geogrid interaction problems including geogrid pullout test, strip footing on geogrid-reinforced sand and geogrid reinforced fill over void. The numerical results show the efficiency of the coupled framework to model the interlocking effect between the soil and the geogrid sheet. New insights into the nature of the interaction between the soil and the geogrid at the microscopic scale are also presented.

1 INTRODUCTION

Continuum approaches (e.g., Finite Element and Finite Difference) are generally used for the numerical analysis of soil-structure interaction problems. The finite element method (FE) has proven to be a powerful tool to model both structural elements and the surrounding soil. Although FE can be used efficiently to model the soil behavior at the macroscopic scale, the discontinuous nature of the soil particles is not easy to represent. The discrete element method (DE) proposed by Cundall and Strack (1979) is an alternative approach for the modeling of these systems. While the DE method can efficiently model soil discontinuous behavior (Lobo-

Guerrero and Vallejo; 2006; Tran et al., 2012, 2013a, 2013b), using the DE method to model structural elements can lead to inaccurate responses.

To take advantage of both FE and DE methods, the buried structure can be modeled using FE whereas the soil can be modeled using the DE method. The coupling of the two methods can efficiently model the behavior of both the soil and the structure. In this paper, a coupled Finite-Discrete element (FE-DE) framework that is capable of modeling soil-structure interaction problems at the microscopic scale level is described and used to investigate three selected geogrid-soil interaction problems involving (1) geogrid pullout test, (2) strip footing on geogrid-reinforced sand and (3) geogrid reinforced fill over void. Modeling of these problems allows for the merits of the soil-geogrid interaction to be investigated.

2 COUPLED FINITE-DISCRETE ELEMENT FRAMEWORK

The coupled FE-DE framework used in this study is implemented into an open source discrete element code YADE (Šmilauer et al., 2010) and is briefly described in the following sections.

The FE analysis in the coupled framework is performed using a dynamic relaxation approach (Dang and Meguid, 2010, 2013). The interaction between DE particles is a dynamic process using a time-stepping algorithm with an explicit finite difference scheme. Since dynamic approach is also used in the FE analysis, it is possible to couple the two compatible approaches. In this study, the interaction between two DE particles is represented by normal force $\vec{\mathbf{F}}_N$, tangential force $\vec{\mathbf{F}}_T$ and rolling resistance moment $\vec{\mathbf{M}}_r$. The normal and tangential contact forces are determined using the normal penetration between the two particles $\vec{\boldsymbol{\Delta}}_N$ and incremental tangential displacement $\delta\vec{\boldsymbol{\Delta}}_T$. Normal and tangential stiffnesses of the contact, noted as K_N and K_T, are determined using particle material modulus (E) and particle radius (r). The rolling resistance moment $\vec{\mathbf{M}}_r$ is introduced to represent the rolling restraint between the two particles.

Interface elements are implemented to model the interaction between the FE and DE domains. Triangular facets are used as interface elements. A triangular facet is directly defined by the three nodes of the element located on the interface if the element has a triangular or a tetrahedron shape. In the case of quadrilateral or hexahedral elements, the contact interface is divided into four triangular facets by creating a temporary center node determined by:

$$x^{(O)} = \frac{1}{4}\sum_{i=1}^{4} x^{(i)} \tag{1}$$

where, $x^{(i)}$ is the coordinate of node i of the quadrilateral.

Interaction forces transmitted to FE nodes can be determined:

$$\vec{\mathbf{F}}_i = \vec{\mathbf{F}}_{contact}.N_i \tag{2}$$

where, $\vec{\mathbf{F}}_{contact} = \vec{\mathbf{F}}_N + \vec{\mathbf{F}}_T$ is the total contact force, N_i is the shape functions obtained using the natural coordinates of the contact point.

Different time-steps for each domain are implemented in the coupling framework to improve the computational efficiency. The time-step in the FE domain (Δt_{FE}) is selected as $\Delta t_{FE} = n\Delta t_{DE}$ where, Δt_{FE} is the time-step in the DE domain, *n* is an integer such that $n \le \frac{[\Delta t_{FE}]}{\Delta t_{DE}}$. This algorithm is implemented by executing the FE solver for every *n* DE computations. Calculation steps in a typical cycle are illustrated in Fig. 1.

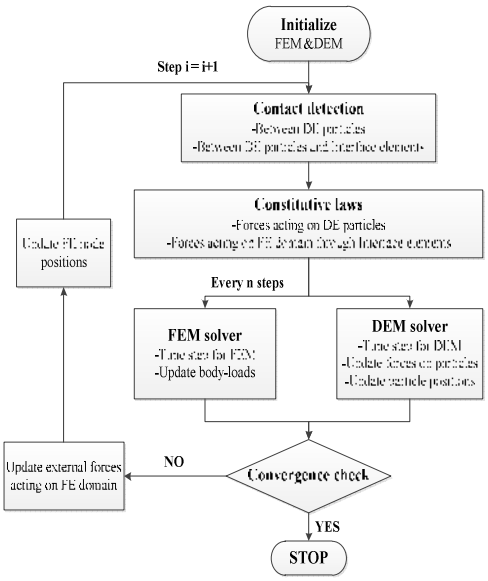

Fig. 1. Flow chart for the coupled Finite - Discrete element method

3 GEOGRID PULLOUT TEST

3.1 Model generation

In this study, an experimental pullout test performed on a geogrid type SS-1 (Alagiyawanna et al., 2001; Sugimoto and Alagiyawanna, 2003) is adopted and numerically modeled using the proposed coupled FE-DE model. Details of the laboratory test are summarized as follows:

The soil container was reported to be 0.68 m in length, 0.3 m in width and 0.62 m in height. The soil used in the experiment was Silica Sand No. 5 with D_{50} = 0.34 mm and a peak friction angle of 29.9^o (D_r = 70%) as obtained from laboratory triaxial tests. A geogrid specimen (Tensar SS-1 with polypropylene material and stiffness 285.6 kN/m at a strain of 3%) of 500 mm in length and 300 mm in width was used throughout the experiments. The sand was placed in layers using raining technique and the pullout load was applied using a clamp attached to the front end of the geogrid sheet. Vertical stresses 49 kPa and 93 kPa were applied at the top and bottom of the box using air bags to prevent vertical movement of the geogrid during the test. The geogrid was pulled out at a constant rate of 1.0 mm/min.

The numerical model has been developed such that it follows the geometry and test procedure used in the actual experiment. The geogrid is modeled using FE while the soil is

modeled using DE. Interface elements are used to simulate the interaction between the two domains. The biaxial SS-1 geogrid is modeled using 8-noded brick elements. A non-deformable clamp is introduced at one end of the geogrid. The initial distance between the front wall and the 1st transverse member is 30 mm assuring all transverse members are still in the soil domain during the test (the maximum pullout displacement is 25 mm). A linear elastic material model is used for the geogrid sheet and its properties are determined by matching the experimental load-displacement curve obtained from the index tests at a medium strain of 2% (as shown in Table 1). The full geometry of the geogrid which comprises over 1300 finite elements and 20,000 interface elements is shown in Fig. 2a. The sand used in the experiment is modeled using spherical DE particles with a mean diameter of 5.1 mm (15 times the real D_{50}) and a standard deviation of 1.0 mm.

Table 1. Input parameters for the pullout test simulation

Type of elements	Parameter	Pullout test	Strip footing on reinforced sand
Discrete particles	Density (kg/m^3)	2640	2650
	Material modulus E (MPa)	100	38
	Ratio K_T/K_N	0.1	0.25
	Coefficient of friction (tan φ)	0.54	0.68
	Rolling resistance coefficient	0.05	0.01
	Damping coefficient	0.2	0.2
Finite elements	Young modulus E (MPa)	2.8E+3	1.4E+3
	Poisson's ratio ν	0.3	0.3
Interface elements	Material modulus E (MPa)	100	38
	Ratio K_T/K_N	0.1	0.25
	Coefficient of friction (tan φ)	0.95	0.42

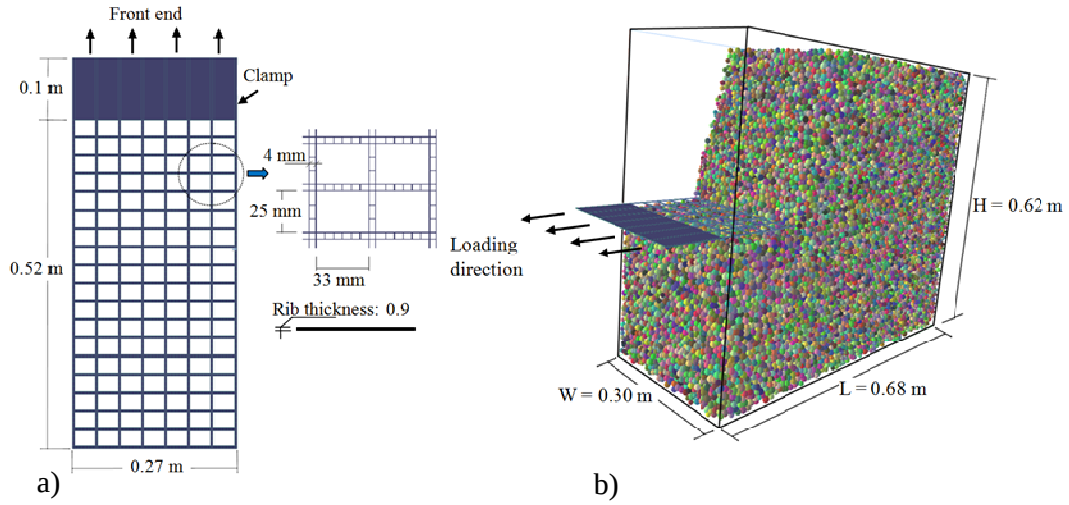

Fig. 2. a) Geometry of the geogrid (pullout test simulation)
b) Initial DE specimen of the pullout test simulation (partial view)

The packing algorithm (Tran et al. 2012, 2013a, 2013b) is used to generate the discrete soil sample with a porosity of 0.39. Particle properties are determined by matching the results of the numerical and experimental triaxial test. A summary of the selected parameters is given in Table 1. The 3D geometry of the final sample is partially shown in Fig. 2b.

3.2 Pullout test model

After the final specimen is formed, the input parameters (Table 1) are then assigned to the discrete particles and the finite elements. No friction is used for the interaction between the particles and the box (smooth rigid) to reduce the boundary effects. Parametric studies indicated that the stiffnesses at the interface do not have a significant effect on the pullout test results. Therefore, the stiffnesses of the interface have been assigned the same values as that of the discrete particles. On the other hand, the coefficient of friction between the discrete particles and interfaces was found to affect the overall response of the soil-geogrid system. In this study, the particle-interface coefficient of friction is determined to be 0.95 based on matching the numerical results with experimental data.

Following the above step, the geogrid is allowed to freely deform and the two vertical stresses (σ_v) 49kPa and 93kPa are applied above and below the soil sample. The vertical stress is kept constant during the test using a stress control mechanism. The pullout procedure is numerically performed using a displacement control approach: lateral displacements were applied to the clamp in 12 steps. In each step, the clamp was forced to move with a same rate of the experiment (in simulation time scheme) until an increase of displacement of 2.5mm was reached. The clamp movement was then stopped until convergence conditions are satisfied in both the DE and FE domains. Additional frontal displacements were applied in subsequent steps and the procedure continued until the frontal displacement U_x reached 25 mm.

3.3 Simulation results

The relationship between the pullout force and the frontal displacement is shown in Fig. 3a as obtained from both the experimental and numerical models. The numerical results generally agreed with the experimental data. The pullout force at a given frontal displacement slightly increased as the vertical stress changes from 49 kPa to 93 kPa. Sugimoto and Alagiyawanna (2003) observed a small slippage of the geogrid at both stress levels leading to marginal difference in pullout resistance. Fig. 3b shows the displacement distributions along the geogrid. It can be seen that geogrid displacements decreased with distance from the face. For all examined frontal displacements the geogrid displacement (U_x) occurred within a limited region from the front side to about the middle of the geogrid. Very small displacements were calculated outside this region. Fig. 3b also confirms the agreement between the measured and calculated displacement using the proposed framework.

The tensile force distributions in the longitudinal members for different frontal displacements are illustrated in Fig. 4a. At a given location along the geogrid, the average tensile force (P_{xx}) in all longitudinal members was found to increase with the increase in frontal displacements. For the investigated range of frontal displacements, the force P_{xx} was large near the front end and rapidly decreased towards the middle of the geogrid. Beyond the

middle zone, P_{xx} became negligible due to the insignificant displacement of the geogrid experienced by the rest of the geogrid.

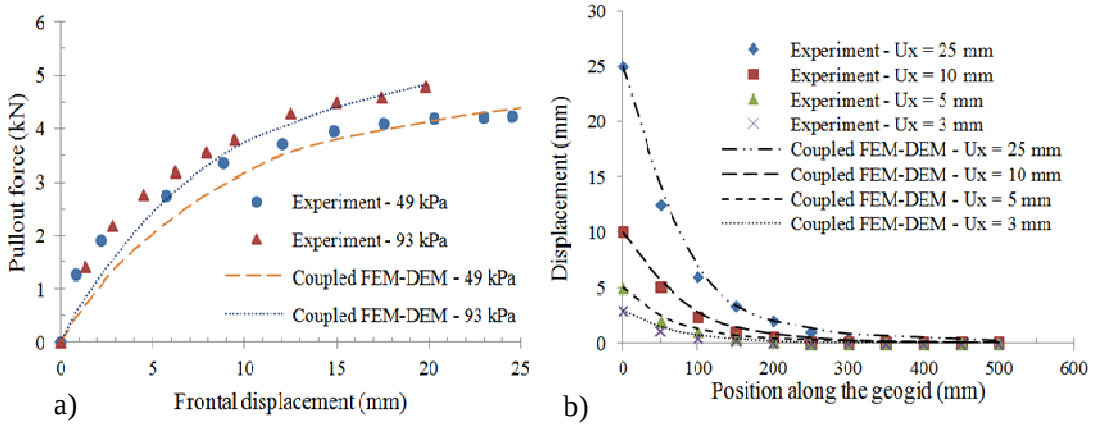

Fig. 3. a) Pullout response of the geogrid
b) Horizontal displacement along the geogrid (σ_v = 49 kPa)

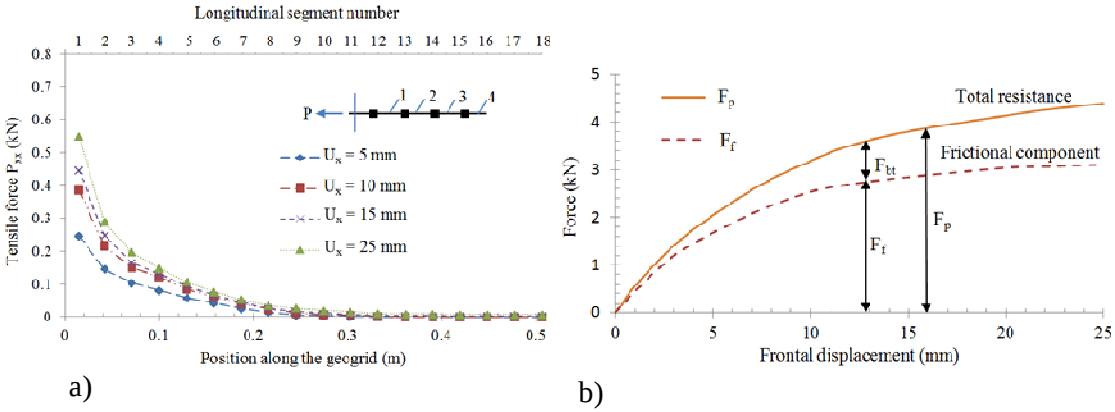

Fig. 4. a) Average tensile force P_{xx} in the longitudinal members (σ_v = 49 kPa)
b) Components of the pullout resistance (σ_v = 49 kPa)

The geogrid comprises longitudinal and transverse members as well as joints connecting these members. Each of these components contributes to the total pullout force. Since the resistance of the joints in this study is numerically included in the frictional resistance of the geogrid, the total pullout resistance F_p can be written as:

$$F_p = F_f + F_{bt} \quad (2)$$

Where F_f is the frictional resistance on the geogrid surface, F_{bt} is the bearing resistance of the transverse members.

Contribution of each component to the total pullout resistance is shown in Fig. 4b. It can be seen that the contribution of the bearing resistance is less than that of the frictional resistance for all considered frontal displacements leading to the frictional component (F_f) dominating

the pullout resistance F_p. However, the rate of increase in F_f became very small when the frontal displacements (U_x) reached about 18 mm as slippage of the geogrid started to develop and most of the shear forces between the particles and interfaces reached their maximum value. The bearing resistance of the transverse elements, on the other hand, shows an increase in value for all examined frontal displacements.

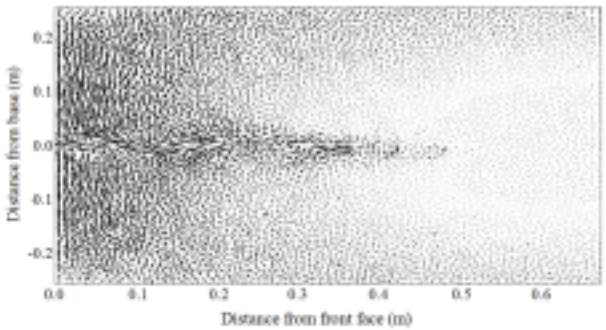

Fig. 5. Displacement field of the soil domain at U_x = 10 mm and σ_v = 49 kPa

Fig. 5 shows the displacement field across the soil domain at a frontal displacement of 10 mm. It can be seen that most of the soil movement developed near the front face of the box leading to soil densification in that area. Soil movement gradually decreased and became negligible around the middle of the geogrid as there is no significant geogrid displacement in this area. Soil in the vicinity of the geogrid tends to move horizontally towards the front face whereas near the front face soil tends to move vertically away from the geogrid. These observations agree well with the results of the X-ray radiographs reported by Alagiyawanna et al. (2001).

3 STRIP FOOTING ON GEOGRID-REINFORCED SAND

3.1 Model generation

Numerical simulation of strip footing on geogrid-reinforced sand using the proposed coupled FE-DE model is conducted based on the experiment reported by Das et al. (1994). In the experiment, the used soil container was 1.1m in length, 0.3m in width and 0.9m in height. The walls were polished to reduce the friction between the soil and the wall. The strip foundation had a width of 76 mm (noted as B) and a length of 300 mm. The soil used in the experiment was medium-grained silica sand with D_{50} = 0.51 mm, average dry unit weight of 17.14 kN/m^3 and a peak friction angle of 41^o (at D_r = 70%) obtained from laboratory direct shear tests. Biaxial geogrids (Tensar SS-0 with PP/HDPE copolymer material and tensile modulus of 182 kN/m at 2% strain) of 760 mm in length and 300mm in width were used in the experiment. The top geogrid layer was installed at a depth 25 mm (0.33B) below the foundation base. The number of geogrid layers installed in soil was varied and the distance between two adjacent layers was 25 mm (0.33B). The sand was placed in layers of 25mm using raining technique. The geogrid layers were placed at predetermined locations. The model foundation was then placed on the soil surface and vertical loading was applied using a hydraulic jack.

Up to two geogrid layers are considered in this study. Interface elements are used to simulate the interaction between the geogrid (modeled using FE) and the soil (modeled using DE). Eight-node brick elements are used to model the geogrid consisting of 11 longitudinal elements and 21 transverse elements. A linear elastic material model is used for the geogrid sheet and its properties are shown in Table 1. The sand is modeled using discrete spherical particles with a mean diameter of 10.2 mm (20 times the real D_{50}) and a standard deviation of 2.0 mm. Soil samples are generated using the gravitational approach proposed by Tran et al. (2012, 2013) to represent the actual soil placement in layers under gravity. Particle properties determined by matching the results of the numerical and experimental direct shear test are shown in Table 1.

After the final specimen is formed, the strip footing (76 mm x 300 mm, Fig. 6a) is numerically generated and initially placed at the surface of the soil layer. The input parameters are then assigned to the discrete particles and the finite elements. A particle-interface coefficient of friction of 0.42 is determined for the simulation to match the experimental results. The geogrids are then allowed to freely deform and pressure at the foundation base is applied in small increments using a stress control mechanism. Each load increment is kept constant until convergence conditions are satisfied in both the DE and FE domains. The foundation pressure is then increased for the next stage.

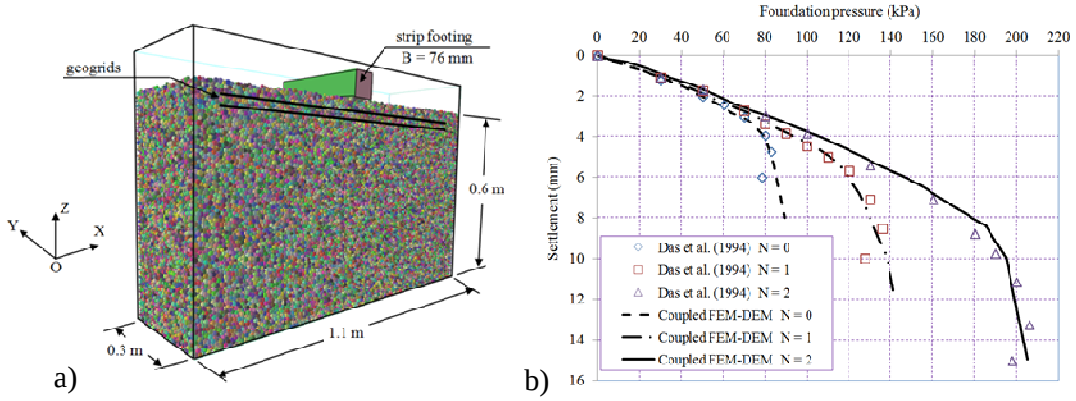

Fig. 6. a) Initial geometry of the geogrid reinforced foundation
b) Load-settlement curves

3.2 Simulation results

The coupled FE-DE simulation results are first compared with the experimental data. Fig. 6b shows the relationship between the foundation pressure and settlement for three cases: no reinforcement (N = 0), one geogrid layer (N = 1) and two geogrid layers (N = 2). It can be seen that the numerical results agreed well with the experimental data for all cases. The ultimate bearing capacity calculated by Das et al. (1994) is consistent with the numerical results. This confirms the agreement between the experiment and numerical simulations using the proposed numerical framework.

The deformed shapes of the geogrid layers for a foundation pressure q = 125 kPa are shown in Fig. 7. The vertical displacement of the geogrid for one reinforcement layer (N = 1) is shown in Fig. 7a whereas the case of two geogrid layers (N = 2) is shown in Fig. 7b. It can

be seen that the vertical displacement of the geogrid for N = 1 is generally larger than that for N = 2. In addition, the vertical displacement of the upper geogrid sheet is larger than that of the lower one. In both cases, the deformations of the geogrids occurred mainly in a region below the foundation and very small deformations were observed outside that region.

The maximum calculated vertical displacements and tensile stresses in the geogrid for different footing pressures are shown in Fig. 8. It is observed that for a given pressure, the vertical displacements and tensile stresses in the geogrid were larger for N = 1 than for N = 2. It is also noted from Fig. 8a and 8b that the deformation and tensile stresses of the upper geogrid layer were generally larger than the lower one for N = 2.

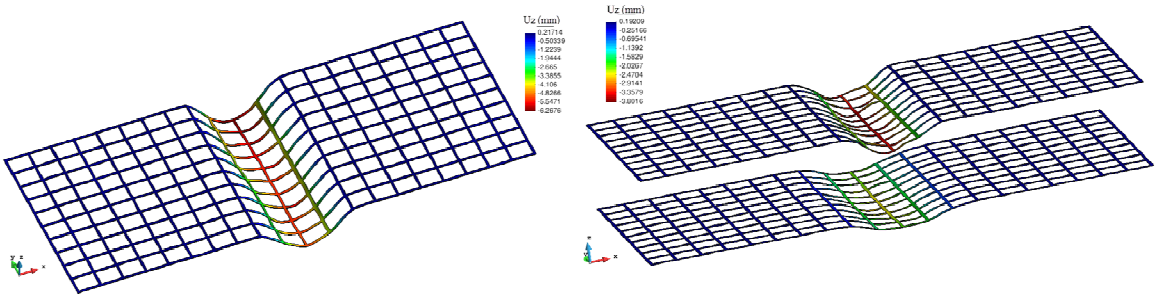

a) b)

Fig. 7. Geogrid vertical displacement at foundation pressure q = 125 kPa.
a) one geogrid layer and b) two geogrid layers

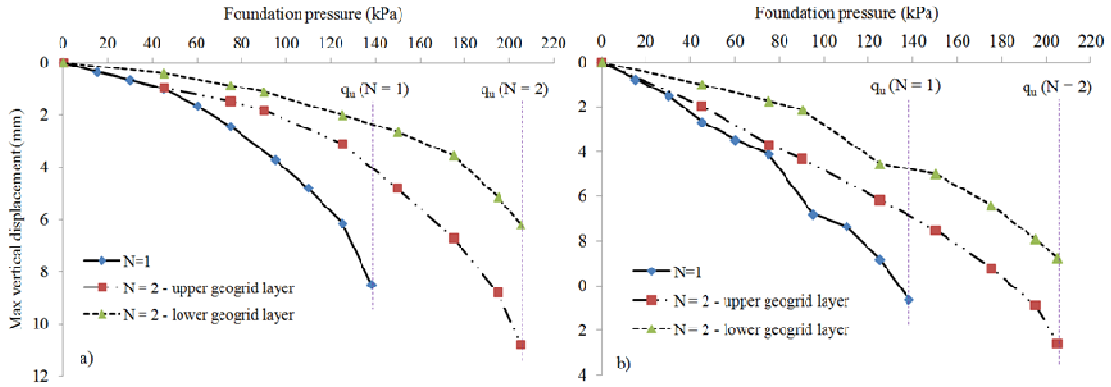

a) b)

Fig. 8. a) Maximum vertical displacements of geogrids
b) Maximum tensile stresses of geogrids

4. GEOGRID REINFORCED FILL OVER VOID

4.1 Model generation

Reinforcement that bridges over voids reduces settlements and protects the overlying earth structures from failure. Kinney and Connor (1987) conducted field tests to investigate the performance of road embankments over voids. Results suggested that geosynthetics can be

beneficial when a fill is placed over voids. In this study, a fill material placed on a geogrid layer overlying an induced void is simulated using the coupled FE-DE framework.

The fill layer has a thickness 0.6m constructed over a natural soil formation and experiences the development of a sudden cavity (width 0.2m and height 0.3m) (Fig. 9a). It is assumed that the void develops in a rigid formation layer and is infinitely long in the out-of-plane direction. The geogrid is installed over a thin soil layer of thickness 0.1m overlying the non-deformable foundation. A surcharge of 5kN/m^2 is applied on top of the fill to simulate surface loading. This surcharge is modeled using a DE layer of thickness 0.05m placed on top of the fill with high density particles. The cavity is assumed to develop after the fill has been constructed. The soil properties used in the previous reinforced foundation problem (Table 1) are also used for the fill material. The geogrid type (Tensar SS-0) from the previous reinforced foundation experiment is also used for the reinforcement.

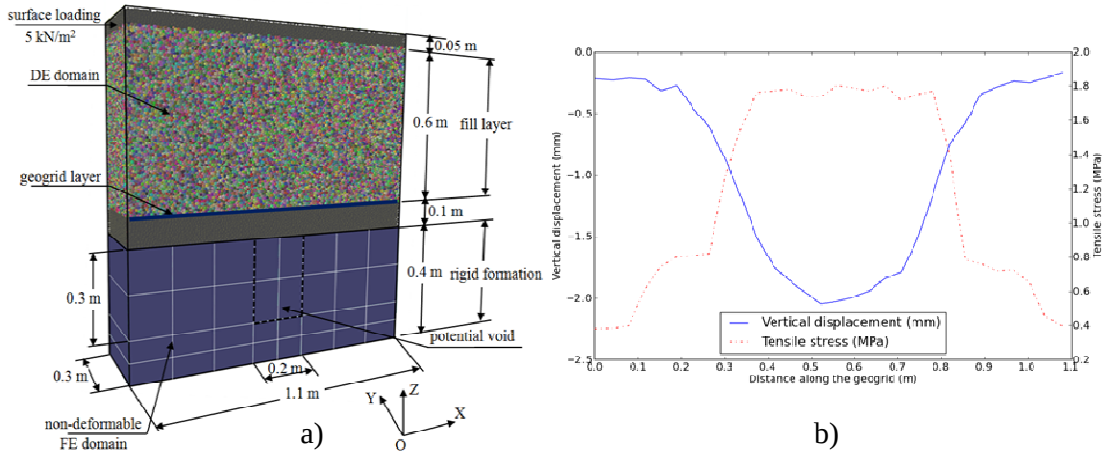

Fig. 9. a) Initial geometry of the geogrid reinforced fill
b) Distributions of vertical displacement and tensile stress along the geogrid due to the induced void

4.2 Simulation results

Distributions of the vertical displacements and tensile stresses along the geogrid are shown in Fig. 9b. It can be seen that the vertical displacements and tensile stresses were small near the two geogrid ends and large at the geogrid center.

The contact orientations in the unreinforced fill are shown in Fig. 10a. It can be seen that with the development of the soil arching within the fill, more contacts were seen in the x direction than in the z direction (xz plane view). This strong anisotropy induced by the soil arching which demonstrated a stronger contact orientation in the horizontal direction than in the vertical direction. The distribution of contacts in the yz plane was elliptical, with the z component being slightly larger than the y component. Meanwhile, quite uniform distribution of the contact orientation was observed in the xy plane. With the placement of a geogrid layer above the void, the distribution of contact orientations in the xz plane of the reinforced fill (Fig. 10b) showed less arching with only a slightly larger value in the horizontal direction compared to the vertical direction. Uniform contact distributions in the yz and xy planes were

also observed. The geogrid reinforcement prevents the rearrangement of contact forces compared to the unreinforced fill with the creation of a void.

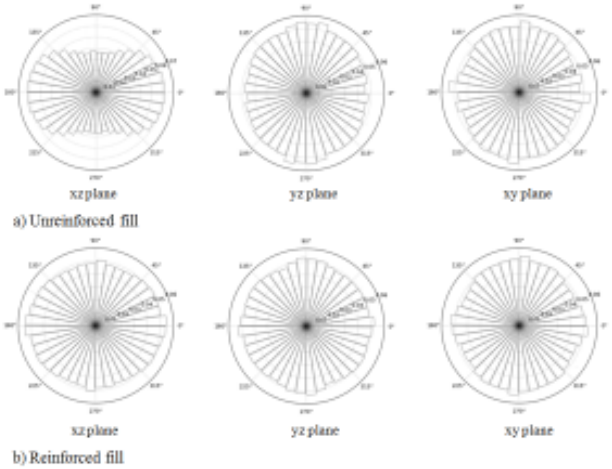

Fig. 10. Distributions of the contact orientation

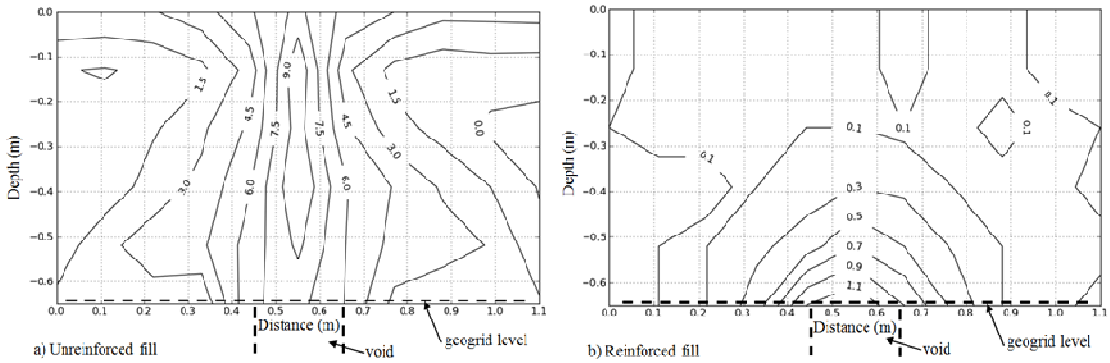

Fig. 11. Percentage porosity changes in the unreinforced and reinforced fills

The soil deformation in the fill layer can be evaluated by analyzing the change in porosity in the soil domain. Using the DE analysis, the change of porosity is obtained by comparing the change in the volume of DE particles within a given volume of dimensions S_x x S_y x S_z = 0.1 m x 0.3 m x 0.1m. The changes in porosity without and with the geogrid reinforcement are shown in Fig. 19a and 19b, respectively. In both cases, there was an increase in porosity corresponding to the volumetric dilation in the fill. Maximum dilations occurred above the void location. Up to 10% of porosity changes were observed in the unreinforced fill while much smaller changes (less than 1.1%) were observed in the geogrid reinforced fill. The volumetric dilation in the fill was also reported by Han et al. (2011).

5 CONCLUSIONS

This study investigated soil-geogrid interaction problems using a coupled FE-DE framework. The soil was modeled using discrete elements while the geogrid was modeled using finite elements. The interaction between the DE and FE domains was ensured by using interface elements. The developed framework was used to investigate three geotechnical engineering problems, geogrid pullout test, strip footing on geogrid-reinforced sand and

geogrid reinforced fill over void. Stresses and displacements in the geogrid, contact orientation, particle movements and change of soil porosity were investigated.

The proposed coupled FE-DE method is proven to be effective in capturing soil-geogrid interactions and analyzing the responses of both the geogrid and the surrounding backfill material.

ACKNOWLEDGEMENTS

This research is supported by a research grant from the Natural Sciences and Engineering Research Council of Canada (NSERC). The financial support provided by McGill Engineering Doctoral Award (MEDA) to the first author is greatly appreciated.

REFERENCES

[1] Alagiyawanna, A.M.N., Sugimoto, M., Sato, S., Toyota, H. Influence of longitudinal and transverse members on geogrid pullout behaviour during deformation. *Geotextiles and Geomembranes* (2001), 19 (8), 483–507.

[2] Cundall. P.A, and Strack O.D.L. A discrete numerical model for granular assemblies. *Géotechnique* (1979), 29(1): 47-65.

[3] Dang, H.K., and Meguid, M.A. Evaluating the performance of an explicit dynamic relaxation technique in analyzing non-linear geotechnical engineering problems. *Computers and Geotechnics* (2010), 37(1), 125-131.

[4] Dang, H.K., and Meguid, M.A. An efficient finite-discrete element method for quasi-static nonlinear soil-structure interaction problems. *International Journal for Numerical and Analytical Methods in Geomechanics* (2013), 37(2), 130-149.

[5] Das, B.M., Shin, E.C., and Omar, M.T. The bearing capacity of surface strip foundations on geogrid-reinforced sand and clay—a comparative study. *Geotechnical and Geological Engineering* (1994), 12(1), 1-14.

[6] Han, J., Bhandari, A., and Wang, F. DEM Analysis of Stresses and Deformations of Geogrid-Reinforced Embankments over Piles. *International Journal of Geomechanics* (2011), 12(4), 340–350.

[7] Kinney, T.C., and Connor, B. Geosynthetics supporting embankments over voids. *Journal of cold regions engineering* (1987), 1(4), 158-170.

[8] Lobo-Guerrero, S., and Vallejo, L.E. Discrete element method analysis of railtrack ballast degradation during cyclic loading. *Granular Matter* (2006), 8(3), 195-204.

[9] Šmilauer, V., Catalano, E., Chareyre, B., Dorofeenko, S., Duriez, J., Gladky, A., Kozicki, J., Modenese, C., Scholtès, L., Sibille, L., Stránský, J., and Thoeni, K. Yade Documentation. *The Yade Project, 2010.* (http://yade-dem.org/doc/).

[10] Sugimoto, M., Alagiyawanna, A.M.N., Kadoguchi, K. Influence of rigid and flexible face on geogrid pullout tests, *Geotextiles and Geomembranes* (2001), 19 (5), 257–277.

[11] Tran, V.D.H., Meguid, M.A., and Chouinard, L.E. Discrete Element and Experimental Investigations of the Earth Pressure Distribution on Cylindrical Shafts. *International Journal of Geomechanics* (2012) (in press).

[12] Tran, V.D.H., Meguid, M.A., and Chouinard, L.E. A Finite-Discrete Element Framework for the 3D Modeling of Geogrid-Soil Interaction under Pullout Loading Conditions. *Geotextiles and Geomembranes* (2013), 37, 1-9.

[13] Tran, V.D.H., Meguid, M.A., and Chouinard, L.E. Three Dimensional Analysis of Geogrid Reinforced Soil Using Finite-Discrete Element Framework. *International Journal of Geomechanics* (submitted, 2013).